Proceedings of the 2014 10th International Pipeline Conference
IPC2014
September 29 - October 3, 2014, Calgary, Alberta, Canada

IPC2014-33712

RELATIONSHIP BETWEEN *J* AND CTOD IN SE(T) AND SE(B) SPECIMENS FOR STATIONARY AND GROWING CRACKS

Diego F. B. Sarzosa
Department of Naval Architecture and Ocean Engineering
University of São Paulo, São Paulo, Brazil
E-mail: dsarzosa@usp.br

Claudio Ruggieri
Department of Naval Architecture and Ocean Engineering
University of São Paulo, São Paulo, Brazil
E-mail: claudio.ruggieri@usp.br

ABSTRACT

Current defect assessment procedures of large engineering structures, including pipeline systems and their welded components such as field girth welds, employ crack growth resistance curves in terms of *J*-resistance or CTOD-resistance curves. Standardized techniques for crack growth resistance testing of structural steels are based upon laboratory measurements of load-displacement records and adopt two related estimation formulas for fracture toughness values: 1) estimating *J* from plastic work based on crack mouth opening displacement (CMOD), and 2) determining the CTOD value from first evaluating the plastic component of *J* using the plastic work defined by the area under the load vs. CMOD curve and then converting it into the corresponding value of plastic CTOD. This work addresses an investigation on the relationship between *J* and CTOD for three-point SE(B) and clamped SE(T) fracture specimens based upon extensive numerical analyses conducted for crack configurations with varying crack sizes. These analyses include stationary and crack growth plane-strain results to determine *J* and CTOD for the cracked configurations based on load-displacement records. The numerical computations show strong similarities between the *J*-CTOD relationship for stationary and growth analysis with important implications for experimental measurements of CTOD-resistance curves. The study provides a body of results which enables establishing accurate relationships between *J* and CTOD for use in testing protocols for toughness measurements.

INTRODUCTION

Fracture assessments in the upper-shelf of ferritic steels remain a key issue for the safety and fitness-for-service (FFS) analyses of critical structures, including piping systems and marine facilities. Structural steels generally exhibit significant increases in fracture toughness over the first few mm of stable crack extension as conventionally characterized by crack growth resistance ($J-\Delta a$ or, equivalently, CTOD $-\Delta a$) curves (also termed *R*-curves); here, the *J*-integral or the crack-tip opening displacement (CTOD) describes the intensity of near-tip deformation [1, 2] and Δa is the amount of crack growth. Fracture mechanics based approaches to analyze ductile fracture in structural components rely upon the notion that a single *R*-curve, independent of specimen geometry, characterizes the fracture resistance of the material [1, 2]. In particular, Engineering Critical Assessment (ECA) procedures applicable to reeled pipes [3] rely on direct applications of *J*-resistance data measured using small, laboratory fracture specimens to specify acceptable flaw sizes. These approaches allow the specification of critical crack sizes based on the predicted growth of crack-like defects under service conditions. Current efforts now underway [4, 5, 6, 7, 8, 9] advocate the use of single edge notch tension specimens (often termed SE(T) crack configurations) to measure experimental *R*-curves more applicable to high pressure piping systems and girth welds of marine steel risers. Here, the SE(T) geometry generally develops low levels of crack-tip stress triaxiality (associated

with the predominant tensile loading which develops during the fracture test) thereby contrasting sharply to conditions present in deeply cracked SE(B) and C(T) specimens. Recent applications of SE(T) fracture specimens to characterize crack growth resistance properties in pipeline steels [10] have been effective in providing larger flaw tolerances while, at the same time, reducing the otherwise excessive conservatism which arises when measuring the material's fracture toughness based on high constraint, deeply-cracked, SE(B) specimens.

To the extent that J describes the crack-tip conditions with increased crack extension and, further, that a unique $J-\text{CTOD}$ relationship holds true for stationary and growing cracks, both $J-\Delta a$ and $\text{CTOD}-\Delta a$ curves equally characterize the crack growth resistance behavior for the tested material. However, because of the widespread use of the CTOD parameter since its introduction in the 70s, when early development conducted at the Welding Institute introduced the concept of a CTOD design curve [11, 12], current defect assessment procedures adopted by the oil and gas industry favor the utilization of $\text{CTOD}-R$ curves rather than J-resistance measurements. A widely employed standardized technique in experimental measurements of CTOD for structural steels derives from BS7448 [13] which essentially determines the crack tip opening displacement for a deeply cracked bend specimen based upon a simple plastic hinge model to correlate the crack mouth opening displacement (CMOD) with CTOD. While this approach has proven highly effective, albeit with questionable accuracy, in fracture testing of structural steels and their weldments, it is not necessarily applicable nor very practical for experimental measurements of CTOD using SE(T) specimens.

Recent revisions of ASTM E1820 [14] and ISO 15653 [15] evaluate the crack tip opening displacement (CTOD) from experimentally measured records of load vs. crack mouth opening displacement (CMOD) applicable to only C(T) and SE(B) fracture specimens. These procedures now determine the CTOD value from first evaluating the plastic component of J using the plastic work defined by the area under the load vs. CMOD curve and then converting it into the corresponding value of plastic CTOD. The approach has the potential to simplify evaluation of CTOD-values while, at the same time, relying on a rigorous energy release rate definition of J for a cracked body. In particular, the methodology can be extended in straightforward manner to evaluate the CTOD in SE(T) specimens from experimentally measured load vs. CMOD records provided accurate relationships between J and CTOD for this crack configuration are known.

This work addresses an investigation on the relationship between J and CTOD for three-point SE(B) and clamped SE(T) fracture specimens based upon extensive numerical analyses conducted for crack configurations with varying crack sizes. These analyses include stationary and crack growth plane-strain results to determine J and CTOD for these cracked configurations based on load-displacement records. Laboratory testing of an API 5L X70 steel at room temperature using standard, deeply cracked C(T) specimens is used to measure the crack growth resistance curve for the material and to calibrate the key microstructural parameter utilized in the growth analysis. The numerical computations show strong similarities between the J-CTOD relationship for stationary and growth analysis with important implications for experimental measurements of CTOD-resistance curves. The study provides a body of results which enables establishing accurate relationships between J and CTOD for use in testing protocols for toughness measurements.

J AND CTOD EVALUATION PROCEDURE

J Estimation Procedure Based on Plastic Work

Evaluation of the J-integral from laboratory measurements of load-displacement records is most often accomplished by considering the elastic and plastic contributions to the strain energy for a cracked body under Mode I deformation [2] as follows

$$J = J_e + J_p \tag{1}$$

where the elastic component, J_e, is given by the standard form

$$J_e = \frac{K_I^2}{E'} \tag{2}$$

in which K_I is the (Mode I) elastic stress intensity factor and $E' = E$ or $E' = E/(1-\nu^2)$ whether plane stress or plane strain conditions are assumed with E representing the (longitudinal) elastic modulus. Here, solutions for the elastic stress intensity factor, K_I, for a SE(B) specimen are given by Tada et al. [16] whereas Cravero and Ruggieri [17] provide wide range K_I-solutions for pin-loaded and clamped SE(T) specimens.

The plastic component, J_p, is conveniently evaluated from the plastic area under the load-CMOD curve as

$$J_p = \frac{\eta_J A_p}{bB} \tag{3}$$

where A_p is the plastic area under the load-CMOD curve and factor η_J represents a nondimensional parameter which describes the effect of plastic strain energy on the applied J. The previous definition for J_p derives from the assumption of nonlinear elastic material response thereby providing a deformation plasticity quantity. Figure 1 schematically illustrates the procedure to determine the plastic area to calculate J from typical load-CMOD records in which the crack mouth opening displacement is often also denoted as V.

CTOD Evaluation Procedure

The previous framework also applies when the CTOD is adopted to characterize the crack-tip driving force. Following the earlier analysis for the J-integral and using the connection between J and the crack-tip opening displacement (δ) [18, 19] given by

$$\delta = \frac{J}{m\sigma_{ys}} \tag{4}$$

in which m is a dimensionless constant, a formally similar expression to Eq. (1) is employed to yield

$$\delta = \delta_e + \delta_p \tag{5}$$

where the elastic component, δ_e, is given by

$$\delta_e = \frac{K_I^2}{m_{SSY}\sigma_{ys}E'} \tag{6}$$

and the plastic component, δ_p, is expressed as

$$\delta_p = \frac{\eta_\delta A_p}{bB\sigma_{ys}} \tag{7}$$

where factor η_δ now represents a nondimensional parameter which describes the effect of plastic strain energy on the applied CTOD. In the above expressions, m_{SSY} is a plastic constraint factor relating J and CTOD under small scale yielding [2], σ_{ys} denotes the material's yield stress and parameter m represents a proportionality coefficient often used to relate the total value of J to the total value of CTOD which strongly depends on the material strain hardening [18, 19].

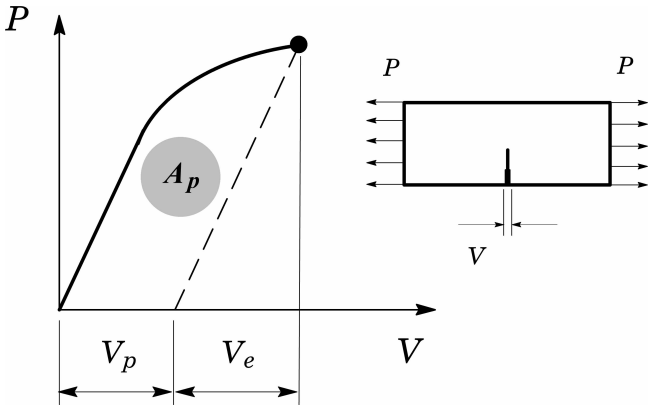

Figure 1: Plastic area under the load-displacement (CMOD) curve for a fracture specimen.

NUMERICAL PROCEDURES

Finite Element Models for Stationary Crack Analyses

Nonlinear finite element analyses are described for plane-strain models of bend and tension loaded crack configurations covering 1-T plane-sided SE(B) and SE(T) fracture specimens with fixed overall geometry having thickness B =25.4 mm and varying crack sizes. The analysis matrix includes standard SE(B) specimens ($S/W = 4$) and clamped SE(T) specimens ($H/W = 10$) with $W/B = 2$ having $a/W = 0.10$ to 0.7 with increments of 0.05. Here, a is the crack size, W is the specimen width, S defines the specimen span for the bend configuration and H represents the distance between clamps for the tension specimen. Figure 2 shows the geometry and specimen dimensions for the analyzed crack configurations. Since the J-CTOD relationship developed later in the article is strongly dependent on the a/W-ratio (rather than other absolute specimen dimensions, such as W or B), the results described in this investigation suffice to characterize the J-CTOD relationships for SE(B) and clamped SE(T) specimens having different W or B.

Figure 3 shows the finite element models constructed for the plane-strain analyses of the clamped SE(T) specimen having $a/W = 0.5$ for stationary crack analysis. All other crack models have very similar features. A conventional mesh configuration having a focused ring of elements surrounding the crack front is used with a small key-hole at the crack tip; the radius of the key-hole, ρ_0, is 2.5 μm (0.0025 mm) to enhance computation of J-values at low deformation levels. Previous numerical analyses [17] reveal that such mesh design provides detailed resolution of the near-tip stress-strain fields which is needed for accurate numerical evaluation of J-values. Symmetry conditions permit modeling of only one-half of the specimen with appropriate constraints imposed on the remaining ligament. A typical half-symmetric model has one thickness layer of 1300 8-node, 3D elements (~2800 nodes) with plane-strain constraints ($w = 0$) imposed on each node. These finite element models are loaded by displacement increments imposed on the loading points to enhance numerical convergence.

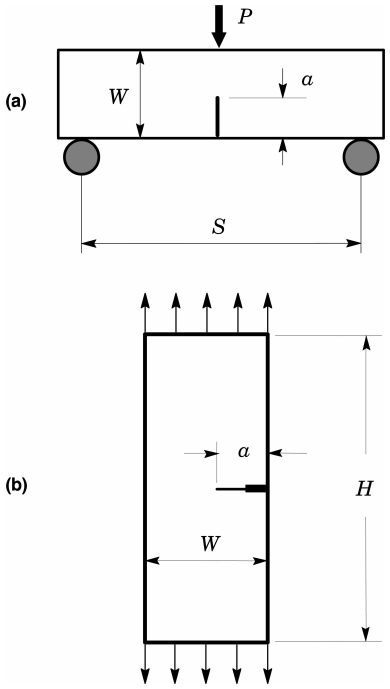

Figure 2: Specimen geometries and dimensions for analyzed crack configurations.

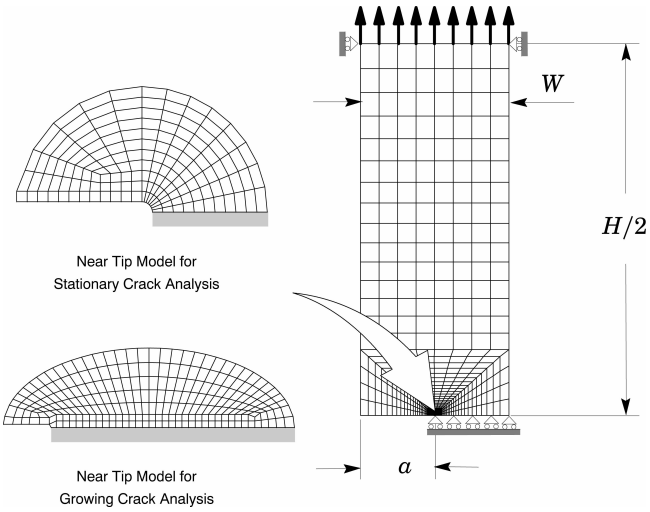

Figure 3: Plane-strain finite element model for the clamped SE(T) specimen with $a/W = 0.5$.

Numerical Models Including Ductile Tearing

Xia and Shih (X&S) [20] proposed an engineering approach based upon damage mechanics to predict *R*-curves for cracked configurations under ductile regime. Material separation occurs through a local fracture mechanism described by the micromechanics parameters D, which defines the thickness of the computational cell layer on which Mode I growth evolves and the initial cell porosity, f_0, which roughly represents the actual metallurgical features of the material. Progressive void growth and subsequent macroscopic material softening in each cell are described by a constitutive model for dilatant plasticity given by Progressive void growth and subsequent macroscopic material softening in each cell are described with the Gurson-Tvergaard (GT) constitutive model for dilatant plasticity [21, 22] given by

$$\left(\frac{\sigma_e}{\bar{\sigma}}\right)^2 + 2q_1 f \cosh\left(\frac{3q_2\sigma_m}{2\bar{\sigma}}\right) - \left(1 - q_3 f^2\right) = 0 \qquad (8)$$

where σ_e denotes the effective Mises (macroscopic) stress, σ_m is the mean (macroscopic) stress, $\bar{\sigma}$ is the current flow stress of the cell matrix material and f defines the current void fraction. Here, factors q_1, q_2 and $q_3 = q_1^2$ are material constants. Using an experimental $J-\Delta a$ curve obtained from a conventional, deeply cracked SE(B) or C(T) specimen, a series of finite element analyses of the specimen is conducted to calibrate values for the cell parameters D and f_0 which bring the predicted $J-\Delta a$ curve into agreement with experiments as described later in the article. Readers are referred to the works of Xia and Shih [20], Ruggieri and Dodds (R&D) [23] and Gullerud et al. [24] for further details.

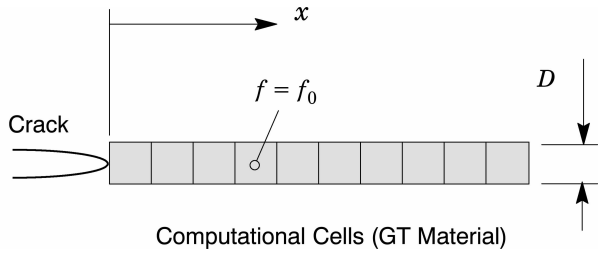

Figure 4: Computational cell model for ductile tearing.

To simulate ductile crack extension using the GT model, the planar meshes (2-D) for the SE(T) and SE(B) fracture specimens are similar to the plane-strain finite element models for stationary crack analyses described previously but contains a row of 60 computational cells along the remaining crack ligament $(W-a)$ as depicted in Fig. 4. Experience with past finite element analyses of fracture specimens to estimate the cell size for common structural and pressure vessel steels suggests values of $50 \sim 200\,\mu$m for D [23, 24, 25]. Here, the cell size is adopted as $D/2 = 100\,\mu$m. This size provides an approximate correlation of spacing between the large inclusions and the crack tip opening displacement (CTOD) at the onset of macroscopic crack growth in conventional fracture specimens for common pressure vessel steels while, at the same time, providing adequate resolution of the stress-strain fields in the active layer and in the adjacent background material.

Calibration of the initial material porosity (void fraction), f_0, for the GT material requires a crack growth analysis to match *R*-curves obtained from testing of high constraint, deeply cracked specimens. Hippert [26] tested 1-T compact tension C(T) specimens ($B = 25.4$ mm) with $a/W = 0.65$ and 20% side-grooves (10% each side) to measure ductile tearing properties for the API X70 pipeline steel utilized in this study. The finite element mesh for the growth analysis of the deeply-cracked C(T) specimen contains a row of 120 computational cells along the remaining crack ligament $(W-a)$ with fixed size of $D/2 \times D/2$ (see Fig. 4). The initially blunted crack tip accommodates the intense plastic deformation and initiation of stable crack growth in the early part of ductile tearing. Symmetry conditions permit modeling of only one-half of the specimen with appropriate constraints imposed on the remaining ligament. This half-symmetric, plane-strain model has one thickness layer of 1611 8-node, 3D elements (3522 nodes) with plane-strain constraints ($w = 0$) imposed on each node and displacement increments imposed on the loading point which permits continuation of the analyses once the load decreases during crack growth.

Material Models and Finite Element Procedures

The elastic-plastic constitutive model employed in the stationary crack analyses reported here follows a flow theory with conventional Mises plasticity in small geometry change (SGC) setting. The numerical solutions for fracture specimens and cracked pipes utilize a simple power-hardening model to characterize the uniaxial true stress ($\bar{\sigma}$) *vs.* logarithmic strain ($\bar{\varepsilon}$) in the form

$$\frac{\bar{\varepsilon}}{\varepsilon_0} = \frac{\bar{\sigma}}{\sigma_0}\,,\ \varepsilon \le \varepsilon_0\ ;\ \frac{\bar{\varepsilon}}{\varepsilon_0} = \left(\frac{\bar{\sigma}}{\sigma_0}\right)^n\,,\ \varepsilon > \varepsilon_0 \qquad (9)$$

where σ_0 and ε_0 are the reference (yield) stress and strain, and n is the strain hardening exponent. The finite element analyses consider material flow properties covering typical structural, pressure vessel and pipeline grade steels with E =206 GPa and ν =0.3: $n = 5$ and E/σ_{ys} =800 (high hardening material), $n = 10$ and E/σ_{ys} =500 (moderate hardening material) and $n = 20$ and E/σ_{ys} =300 (low hardening material).

For the crack growth analyses, the mechanical and flow properties for the API 5L X70 pipeline grade steel tested by Hippert [26] are employed to generate the required numerical solutions in large geometry change (LGC) setting. The material has 484 MPa yield stress (σ_{ys}) and 590 MPa tensile strength (σ_{uts}) at room temperature (20°C) with relatively moderate-to-low hardening properties ($\sigma_{uts}/\sigma_{ys} \approx 1.22$). Additional material properties include Young's modulus E =205 GPa and Poisson's ratio ν =0.3. Based on Annex F of API 579 [27], the Ramberg-Osgood strain hardening exponents describing the stress-strain response for the tested API 5L X70 pipeline grade steel is estimated as $n = 13.3$ Further, to describe the evolution of void growth and associated macroscopic material softening in the computational cells, the GT constitutive model given by Eq. (8) is adopted. The background material outside of the computational cells follows a flow theory with the Mises plastic potential obtained by setting $f \equiv 0$ in Eq. (8). The uniaxial true stress-logarithmic strain response for both the background and cell matrix materials follows a piecewise linear approximation to the measured tensile

response for the material at room temperature given in Hippert [26]. Here, we note that, because the cell parameters are calibrated against experimentally measured crack growth resistance curves for the API X70 pipeline steel as described next, use of the piecewise linear approximation to the measured tensile response for the tested material provides more accurate computed *R*-curves. Further, the two adjustment factors in the Gurson yield condition given by Eq. (8) are taken from the work of Faleskog and Shih [28] as $q_1 = 1.43$ and $q_2 = 0.97$.

The finite element code WARP3D [29] provides the numerical solutions for the plane-strain and 3-D simulations reported here including stationary and crack growth analyses implementing the cell model. The research code FRACTUS2D [30] is employed to compute factor η_δ for the SE(B) and clamped SE(T) specimens, and the $J-$CTOD relationships derived from stationary and growing analyses for the analyzed fracture specimens.

Evaluation of the numerical value of CTOD follows the 90° procedure [2] to the deformed crack flanks. To avoid potential problems with the CTOD computation related to the severe mesh deformation at the crack tip, the approach adopted here defines the value of half the crack tip opening displacement as the intercept between a straight line at 45° from the crack tip and a straight line passing through selected nodes at the crack flank as illustrated in Fig. 5(a-b). The straight line defined by the deformed crack flank nodes is obtained by a linear regression of the corresponding nodal displacements. A similar procedure is also used to measure δ during ductile crack growth. While the crack tip remains sharp for a growing crack, the present approach enables measuring the CTOD based on a similar intercept procedure as illustrated in Fig. 5(c) in which the intercept between a straight line at 45° from the *original* crack tip and a straight line passing through selected nodes at the crack flank defines the current value of CTOD. A similar procedure to measure CTOD during ductile crack growth has also been previously adopted by Verstraete [31] and Hellmann and Schwalbe [32]. Others definitions of CTOD during ductile crack growth can be found in Andrews [33].

The present definition for the CTOD makes strong contact with commonly utilized procedures in stationary crack analyses and it is thus highly effective in describing the macroscopic level of crack-tip deformation in terms of crack opening. A somewhat different picture emerges for the growing crack analysis as the CTOD-value is now more dependent on the methodology to define the crack opening with the extending crack. For small crack extensions, the adopted procedure appears adequate to define a growing CTOD whereas it cannot model properly the crack opening for large amounts of ductile tearing. Currently, we consider the correct definition of CTOD for a growing crack an open issue. An investigation along this line is in progress to provide improved *J*-CTOD relationships based on more accurate and realistic definitions for the CTOD.

Calibration of Cell Parameters

Numerical simulation of ductile tearing in the fracture specimens described here begins with calibration of the cell parameters, f_0 and D, for the pipeline steel employed in this study. The cell size D and initial porosity f_0 define the key parameters coupling the physical and computational models for ductile tearing. The measured resistance curve for a deeply cracked C(T) specimen ($a/W = 0.65$) tested by Hippert [26] (see also Hippert and Ruggieri [34]) using the unloading compliance technique is employed to calibrate these parameters. Within the present context, a series of finite element analyses is conducted to calibrate the cell parameters which establish agreement between the predicted $J-\Delta a$ curve and experiments for a high constraint fracture specimen.

Figure 6 displays the measured crack growth resistance curve (average of two tests) in the TL orientation (described by the solid symbols in the plot) for the tested pipeline steel at room temperature. This fracture data was obtained using conventional 1-T C(T) specimens having the following dimensions: gross thickness, $B = 25$ mm, net thickness, $B_n = 20$ mm (20% side groove), width, $W = 50$ mm, $a = 32.5$ mm ($a/W = 0.65$). Hippert and Ruggieri [34] provide additional details of the material properties, including metallurgical characterization, and the fractures tests.

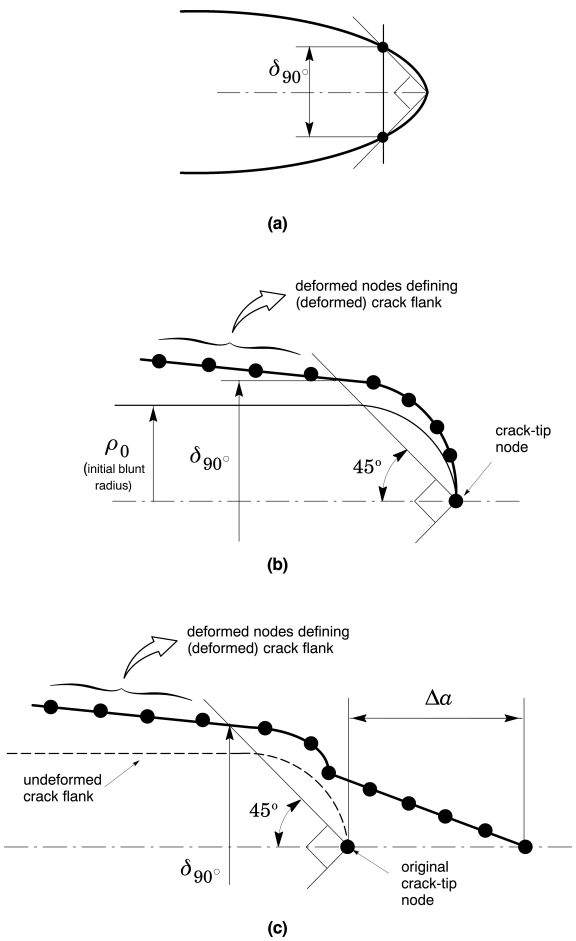

Figure 5: a) Definition of CTOD based on the 90° intercept procedure; b) Adopted numerical strategy to evaluate the CTOD for the stationary crack; c) Adopted numerical strategy to evaluate the CTOD for the growing crack.

As described earlier, we specify the cell size $D/2 = 100\ \mu$m

for the API X70 material employed in this study. Hence, with parameter D fixed, the calibration process then focuses on determining a suitable value for the initial volume fraction, f_0, that produces the best fit to the measured crack growth data for the deeply cracked C(T) specimen. Figure 6 also shows the predicted $J-\Delta a$ curves for this specimen. Predicted R-curves are shown for three values of the initial volume fraction, f_0 =0.0005, 0.00075 and 0.001. For $f_0 = 0.0005$, the predicted R-curve agrees well with the measured values for almost the entire range of growth, albeit lying a little above the measured data for $\Delta a \leq 1$ mm in the blunting line region. In contrast, the use of $f_0 = 0.001$ produces a much lower resistance curve relative to the measured data. Consequently, the initial volume fraction $f_0 = 0.0005$ is thus taken as the calibrated value for the API 5L-X70 steel used subsequently in this study.

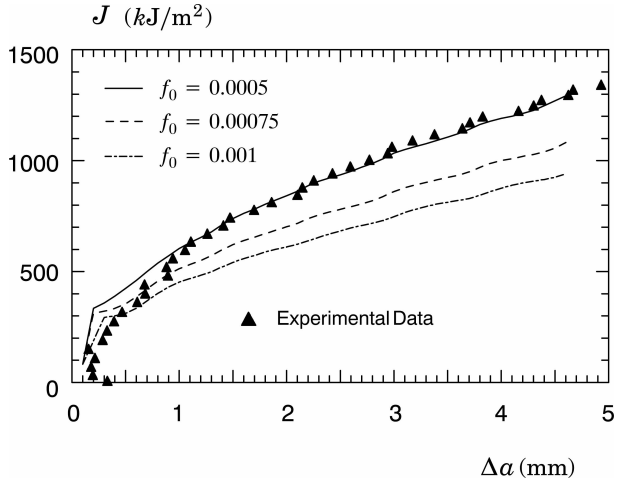

Figure 6: Comparison of measured and predicted R-curve with different f_0-values for side-grooved 1-T C(T) specimen of API 5L-X70 at room temperature.

RESULTS

Plane-Strain η-Factors to Evaluate CTOD

Figures 7 and 8 provide the η_δ-factors to determine the CTOD for the SE(B) and clamped SE(T) specimens with varying a/W-ratios and strain hardening exponents derived from the plane-strain analyses previously described. Here, the η_δ-values depend rather strongly on the hardening exponent, n. This feature can be simply explained in terms of the relationship between J and CTOD given by previous Eq. (4) coupled with definition of factor η_δ described by Eq. (7). Because the material's yield stress, which enters directly into Eq. (4), is dependent on the adopted strain hardening exponent (as previously defined), the η_δ-values are also sensitive to the hardening properties.

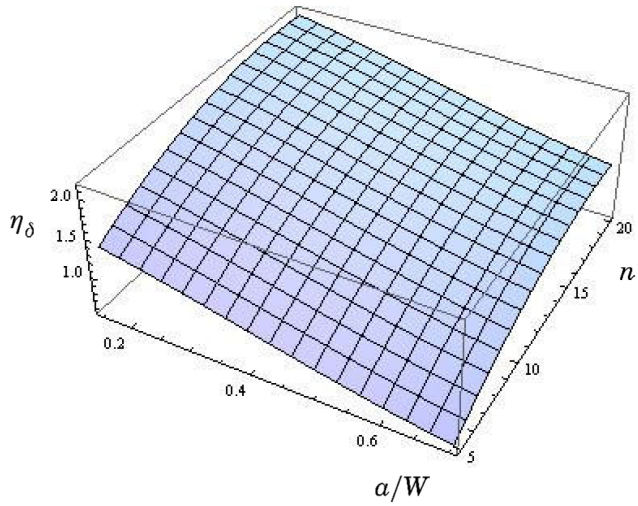

Figure 7: Variation of factor η_δ with a/W-ratio and strain hardening exponent, n, for the analyzed SE(B) specimens.

To provide a simpler manipulation of the previous results aiming at developing testing practices and using the plots displayed in Figs. 7 and 8 for guidance, a functional dependence of factor η_δ with crack size, a/W, and hardening exponent, n, is constructed in the form

$$\eta_\delta = g_1(a/W) + g_2(n) \tag{10}$$

where

$$g_1^{SEB} = 0.833 - 0.544(a/W) - 3.095(a/W)^2 + 2.647(a/W)^3 \tag{11}$$

$$g_2^{SEB} = 0.162n - 0.004n^2 \tag{12}$$

and

$$g_1^{SET} = -0.046 + 1.04(a/W) - 3.15(a/W)^2 + 2.009(a/W)^3 \tag{13}$$

$$g_2^{SET} = 0.072n - 0.002n^2 \tag{14}$$

where it is understood that a multivariate polynomial fitting is adopted to describe the coupled dependence of factor η_δ on the a/W-ratio and hardening exponent. The above expressions are valid in the range $0.2 \leq a/W \leq 0.7$ and $5 \leq n \leq 20$.

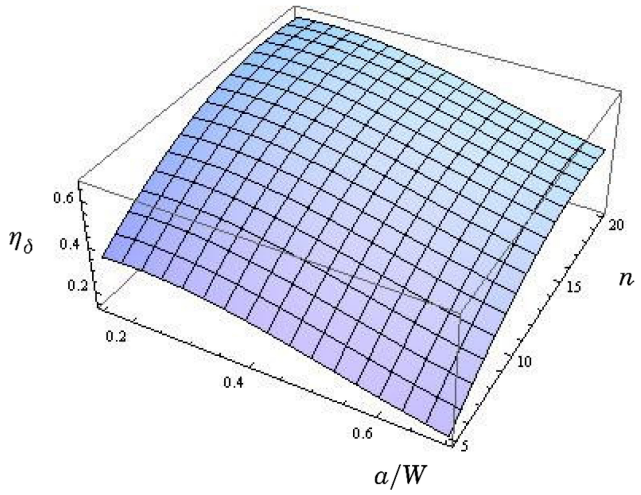

Figure 8: Variation of factor η_δ with a/W-ratio and strain hardening exponent, n, for the analyzed clamped SE(T) specimens.

J-CTOD Relationship in Stationary Cracks

Figures 9-10 provide the variation of the J-integral with CTOD for the SE(B) and clamped SE(T) fracture specimens with different a/W-ratios and the moderate strain hardening material ($n = 10$). The trends and results described here are essentially similar for other strain hardening materials; to conserve space, these results are not shown here.

Consider first the J-CTOD relationship for the SE(B) geometry displayed in Fig. 9(a). It can be seen that the J -CTOD relationship is relatively sensitive to a/W-ratio with increased levels of loading as measured by increased values of J. Figure 9(b) shows the evolution of parameter m with increased J for the analyzed SE(B) specimens. Here, the m-values display a strong variation at small levels of loading (as characterized by small J-values); such behavior derives directly from a strong nonlinear relationship between J and CTOD early in the loading of the specimen. After this transitional behavior, the m-values increase slowly with increased J and attain a constant value, albeit slightly dependent on the a/W-ratio, for larger levels of loading. Consider next the J-CTOD relationship for the clamped SE(T) specimen displayed in Fig. 10(a). In contrast to the previous results, observe that the J-CTOD relationship for the clamped SE(T) geometry is essentially independent of the a/W-ratio. As a consequence, after a transitional behavior at early stages of loading, parameter m for this crack configuration attains a constant value of ~ 1.65 for the entire range of a/W-ratio.

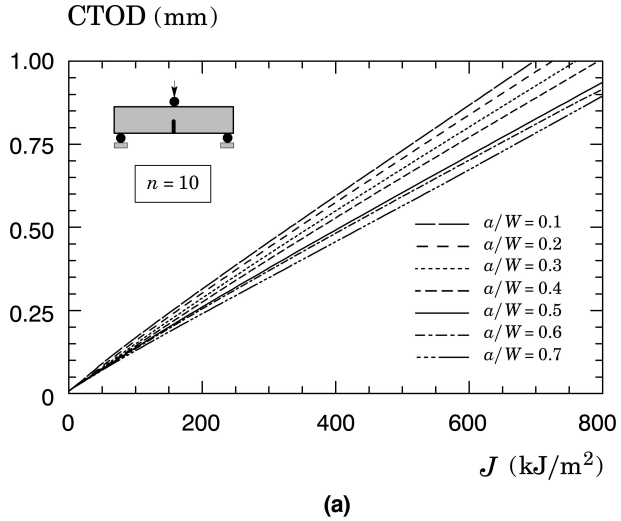

Figure 9: J-CTOD relationship for the SE(B) specimen with varying a/W-ratio and $n = 10$ material derived from stationary crack analysis.

Figures 11 and 12 provide the m-values to determine the CTOD for the SE(B) and clamped SE(T) specimens with varying a/W-ratios and strain hardening exponents derived from the plane-strain analyses previously described. To provide a simpler manipulation of the results displayed in Figs. 11 and 12, a functional dependence of parameter m with crack size, a/W, and hardening exponent, n, is obtained in the form

$$m = h_1(a/W) + h_2(n) \tag{15}$$

where

$$h_1^{SEB} = -0.194 + 1.077(a/W) - 0.238(a/W)^2 \tag{16}$$

$$h_2^{SEB} = 14.391n^{-1} + 0.036n \tag{17}$$

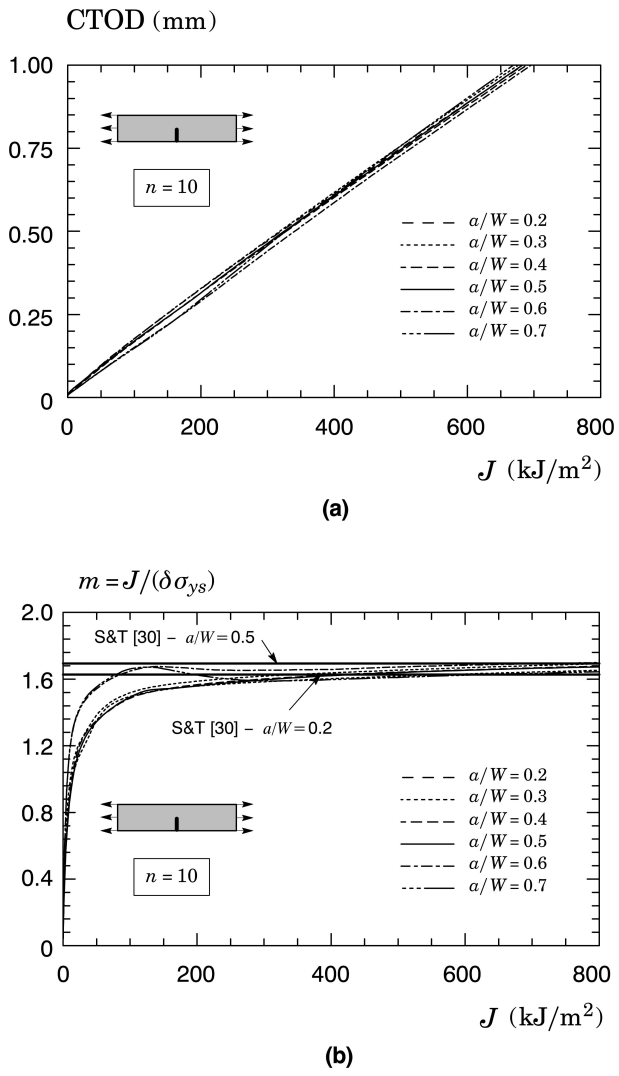

Figure 10: J-CTOD relationship for the clamped SE(T) specimen with varying a/W-ratio and $n = 10$ material derived from stationary crack analysis.

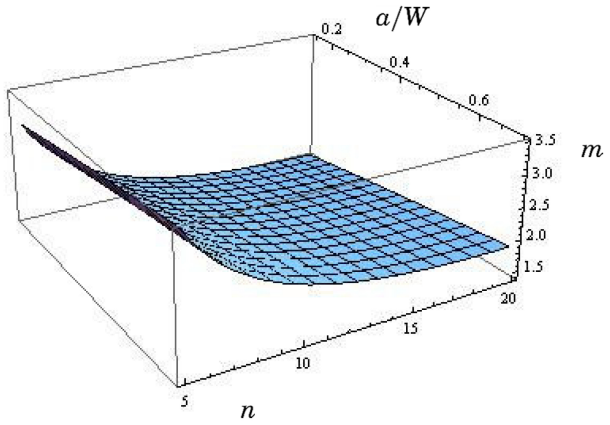

Figure 11: Variation of parameter m with a/W-ratio and strain hardening exponent, n, for the analyzed SE(B) specimens.

and

$$h_1^{SET} = 0.243 - 0.519(a/W) + 0.742(a/W)^2 \qquad (18)$$

$$h_2^{SET} = 11.545n^{-1} + 0.029n \qquad (19)$$

where it is understood that a multivariate polynomial fitting is adopted to describe the coupled dependence of factor η_δ on the a/W-ratio and hardening exponent. The above expressions are valid in the range $0.2 \leq a/W \leq 0.7$ and $5 \leq n \leq 20$.

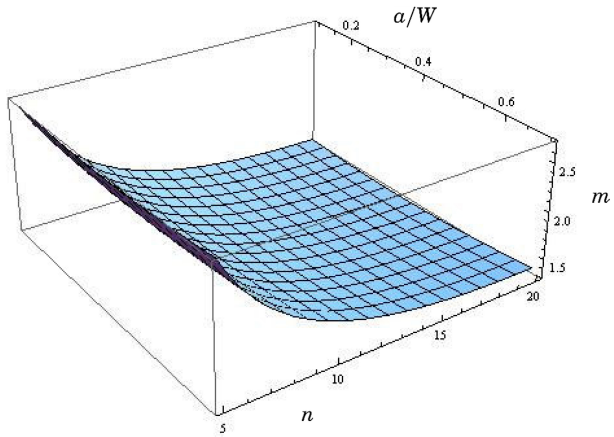

Figure 12: Variation of parameter m with a/W-ratio and strain hardening exponent, n, for the analyzed SE(T) specimens.

To facilitate comparisons with previous reported results for J-CTOD relationships in clamped SE(T) specimens, Fig. 10 also includes the m-values derived from previous Eq. (15) for this crack configuration with $a/W = 0.2$ and 0.5 using the strain hardening exponent of $n = 13.3$ for the API X70 material employed in the numerical analyses. Figure 10 displays m-values derived from 3-D analyses of clamped SE(T) specimens performed by Shen and Tyson (S&T) [35]. It can be seen an overall good agreement between the presents results and the reported m-values from Shen and Tyson (S&T) [35].

J-CTOD Relationship in Growing Cracks

We now direct attention to the evolution of CTOD with J with increased amounts of ductile tearing, Δa, for the analyzed crack configurations. The extensive finite element analyses of SE(B) and SE(T) fracture specimens that include the effects of crack growth provide a basis to compare the J-CTOD relationship in growing cracks with the variation of J with CTOD for stationary cracks. Here, we adopt the API 5L X70 pipeline grade steel tested by Hippert [26] and described previously to compute crack growth resistance curves for these specimens which in turn serve to determine the CTOD for the advancing crack.

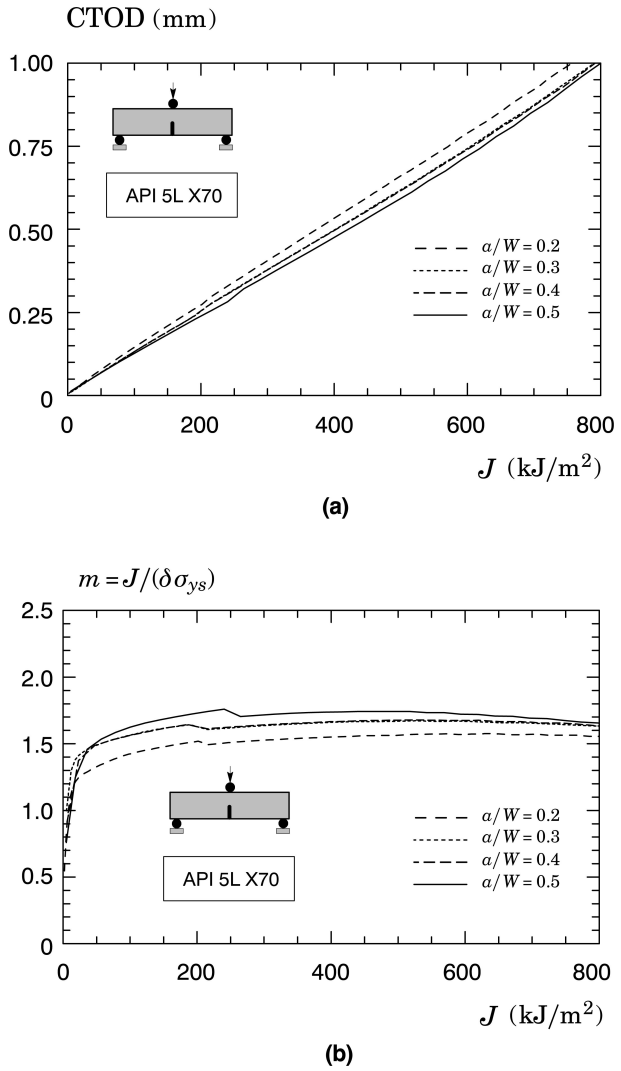

Figure 13: J-CTOD relationship for the SE(B) specimen with varying a/W-ratio and API X70 material derived from the crack growth analysis.

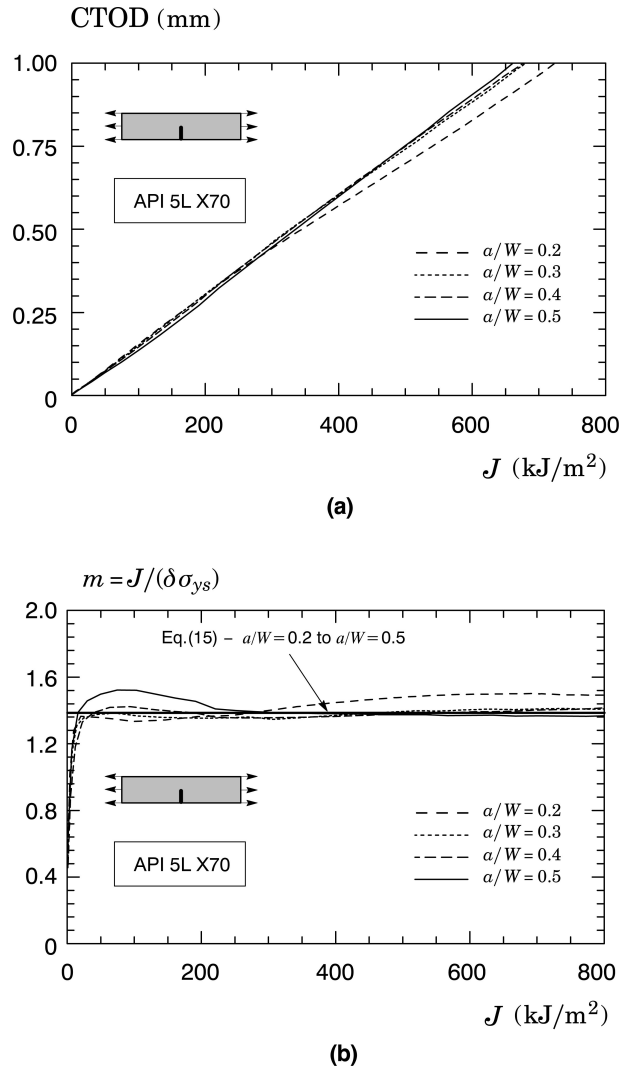

Figure 14: J-CTOD relationship for the clamped SE(T) specimen with varying a/W-ratio and API X70 material derived from the crack growth analysis.

Figures 13-14 provide the variation of the J-integral with CTOD for the SE(B) and clamped SE(T) fracture specimens with different a/W-ratios derived from the crack growth analyses. To facilitate comparisons with the stationary crack results, Fig. 14 also includes the m-values derived from previous Eq. (15) for the SE(T) crack configuration with $a/W = 0.2$ and 0.5 using the strain hardening exponent of $n = 13.3$ for the API X70 material employed in the numerical analyses. The crack growth results clearly reveal a rather weak effect of ductile tearing on the J-CTOD relationships and, consequently, on the evolution of parameter m with increased J for the analyzed fracture specimens. In particular, the m-values derived from a stationary crack analysis for the clamped SE(T) specimen are in very close agreement with the corresponding values derived from the growth analysis.

CONCLUDING REMARKS

The extensive set of nonlinear finite element analyses for detailed plane-strain models of SE(B) and clamped SE(T) fracture specimens with varying crack sizes and straing hardening properties described here provide the basis to determine accurate relationships between J and CTOD for use in testing protocols for toughness measurements. These analyses include stationary and crack growth plane-strain results to determine J and CTOD for SE(B) and clamped SE(T) cracked configurations based on load-displacement records. The results described here clearly reveal a rather weak effect of ductile tearing on the J-CTOD relationships and, consequently, on the evolution of parameter m with increased J for the analyzed fracture specimens. Current procedures to determine CTOD-values from first evaluating the plastic component of J using the plastic work defined by the area under the load vs. CMOD curve and then converting it into the corresponding value of plastic CTOD provide accurate measurements

of crack growth response in terms of CTOD $-R$ curves.

Acknowledgments

This investigation is supported by Fundação de Amparo à Pesquisa do Estado de São Paulo Paulo (FAPESP) through research grant 2012/00094-2 and 2013/01139-2 provided to the first author (DFBS). The work of CR is supported by the Brazilian Council for Scientific and Technological Development (CNPq) through Grants 304132/2009-8 and 476581/2009-5. The authors are indebted to Dr. Eduardo Hippert Jr. (PETROBRAS) for providing the motivation to this work and for the many helpful and insightful discussions on testing protocols for crack growth measurements.

References

[1] J. W. Hutchinson, Fundamentals of the phenomenological theory of nonlinear fracture mechanics, Journal of Applied Mechanics 50 (1983) 1042–1051.

[2] T. L. Anderson, Fracture Mechanics: Fundaments and Applications - 3rd Edition, CRC Press, Boca Raton, FL, 2005.

[3] Det Norske Veritas, Submarine pipeline systems, Offshore Standard OS-F101 (2010).

[4] Det Norske Veritas, Fracture control for pipeline installation methods introducing cyclic plastic strain, DNV-RP-F108 (2006).

[5] S. Cravero, C. Ruggieri, Estimation procedure of J-resistance curves for SE(T) fracture specimens using unloading compliance, Engineering Fracture Mechanics 74 (2007) 2735–2757.

[6] S. Cravero, C. Ruggieri, Further developments in J evaluation procedure for growing cracks based on LLD and CMOD data, International Journal of Fracture 148 (2007) 347–400.

[7] G. Shen, W. R. Tyson, Crack size evaluation using unloading compliance in single-specimen single-edge notched tension fracture toughness testing, Journal of Testing and Evaluation 37 (4) (2009) JTE102368.

[8] H. Tang., K. Minnaar., S. Kirbey., M. Macia, Development of sent test procedure for strain based design of welded pipelines, in: 8th International Pipeline Conference, Calgary, Alberta, Canada, 2010.

[9] D. P. Fairchild, S. Shafrova, H. Tang, W. Cheng, Sent test data for pipeline girth welds, in: 6th Pipeline Techonology Conference, Ostend, Belgium, 2013.

[10] D. Y. Park, W. R. Tyson, J. A. Gianetto, G. Shen, R. S. Eagleson, Evaluation of fracture toughness of X100 pipe steel using SE(B) and clamped SE(T) single specimens, in: 8th International Pipeline Conference (IPC) , Calgary, Canada, 2010.

[11] F. M. Burdekin, M. G. Dawes, The crack opening displacement approach to fracture mechanics in yielding materials, Journal of Strain Analysis 1 (1966) 144–153.

[12] J. D. Harrison, M. G. Dawes, G. L. Archer, M. S. Kamath, The cod approach and its application to welded structures, in: J. D. Landes, J. A. Begley, G. A. Clarke (Eds.), Elastic-Plastic Fracture, ASTM STP 668, American Society for Testing and Materials, Philadelphia, 1979, pp. 606–631.

[13] British Standard, Fracture mechanics toughness tests - Part 1. method for determination of $k$ic, critical ctod and critical j values of metallic materials BS 7448-1:1991 (1991).

[14] American Society for Testing and Materials, Standard test method for measurement of fracture toughness, ASTM E1820-2011 (2011).

[15] International Organization for Standardization, Metallic materials - method of test for the determination of quasistatic fracture toughness of welds, ISO 15653-2010 (2010).

[16] H. Tada, P. C. Paris, G. R. Irwin, The Stress Analysis of Cracks Handbook, 3rd Edition, American Society of Mechanical Engineers, 2000.

[17] S. Cravero, C. Ruggieri, Correlation of fracture behavior in high pressure pipelines with axial flaws using constraint designed test specimens - Part I: Plane-strain analyses, Engineering Fracture Mechanics 72 (2005) 1344–1360.

[18] C. F. Shih, Relationship between the J-integral and the crack opening displacement for stationary and extending cracks, Journal of the Mechanics and Physics of Solids 29 (1981) 305–326.

[19] M. T. Kirk, R. H. Dodds, J and CTOD estimation equations for shallow cracks in single edge notch bend specimens, Journal of Testing and Evaluation 21 (1993) 228–238.

[20] L. Xia, C. F. Shih, Ductile crack growth - I: A numerical study using computational cells with microstructurally-based length scales, Journal of the Mechanics and Physics of Solids 43 (1995) 223–259.

[21] A. L. Gurson, Continuum theory of ductile rupture by void nucleation and growth: Part I - yield criteria and flow rules for porous ductile media, Journal of Engineering Materials and Technology 99 (1977) 2–15.

[22] V. Tvergaard, Material failure by void growth to coalescence, Advances in Applied Mechanics 27 (1990) 83–151.

[23] C. Ruggieri, R. H. Dodds, Numerical modeling of ductile crack growth using computational cell elements, International Journal of Fracture 82 (1996) 67–95.

[24] A. S. Gullerud, X. Gao, R. H. Dodds, R. Haj-Ali, Simulation of ductile crack growth using computational cells: Numerical aspects, Engineering Fracture Mechanics 66 (2000) 65–92.

[25] C. Ruggieri, F. Dotta, Numerical modeling of ductile crack extension in high pressure pipelines with longitudinal flaws, Enginering Structures 33 (2011) 1423–1438.

[26] E. Hippert, Experimental investigation of ductile fracture behavior in API X70 grade pipeline steels and applicability of crack growth resistance curves to predict the burst pressure in longitudinally cracked pipes, Ph.D. thesis, Polytechnic School, University of São Paulo, (In Portuguese) (2001).

[27] American Petroleum Institute, Fitness-for-service, API RP-579-1 / ASME FFS-1 (2007).

[28] J. Faleskog, C. Shih, Cell model for nonlinear fracture analysis - I: Micromechanics calibration, International Journal of Fracture 89 (1998) 355–373.

[29] B. Healy, A. Gullerud, K. Koppenhoefer, A. Roy, S. RoyChowdhury, J. Petti, M. Walters, B. Bichon, K. Cochran, A. Carlyle, J. Sobotka, M. Messner, R. H. Dodds, WARP3D: 3-D dynamic nonlinear fracture analyses of solids using parallel computers, Structural Research Series (SRS 607) UILU-ENG-95-2012, University of Illinois at Urbana-Champaign, http://code.google.com/p/warp3d (2013).

[30] C. Ruggieri, FRACTUS2D: Numerical computation of fracture mechanics parameters for 2-D cracked solids, Tech. rep., University of Sao Paulo (2011).

[31] M. Verstraete, Experimental-numerical evaluation of ductile tearing resistance and tensile strain capacity of biaxially loaded pipelines, Ph.D. thesis (2013).

[32] D. Hellmann, K.-H. Schwalbe, On the experimental determination of CTOD based R-curves, in: K.-H. Schwalbe (Ed.), The Crack Tip Opening Displacement in Elastic-Plastic Fracture Mechanics, Geesthacht, Germany, 1985.

[33] W. R. Andrews, CTOD and J relationship for a growing crack, in: K. Schwalbe (Ed.), The Crack Tip Opening Displacement in Elastic-Plastic Fracture Mechanics, Geesthacht, Germany, 1985.

[34] E. Hippert, C. Ruggieri, Experimental and numerical investigation of ductile crack extension in a high strength pipeline steel, in: ASME 2001 Pressure Vessels & Piping Conference (PVP 2001) , Atlanta, GA, 2001.

[35] G. Shen, W. R. Tyson, Evaluation of CTOD from J-integral for SE(T) specimens, in: Pipeline Technology Conference (PTC 2009) , Ostend, Belgium, 2009.